XXI IMEKO World Congress "Measurement in Research and Industry"
August 30 – September 4, 2015, Prague, Czech Republic

PRIMARY SINUSOIDAL CALIBRATION OF FORCE TRANSDUCERS UP TO 2 KILOHERTZ

Ako Chijioke and Nicholas Vlajic

National Institute of Standards and Technology, Gaithersburg, MD 20899, USA.
ako.chijioke@nist.gov.

Abstract – We report the implementation of a swept-sine dynamic force calibration system at NIST. This system is designed to perform primary calibration of force transducers at frequencies up to 2 kHz and forces up to 2 kN. We demonstrate the use of this system to measure the dynamic sensitivity of a strain-gauge based force transducer up to 2 kHz. The current dominant source of uncertainty in the system is angular motion of the calibration assembly.

Keywords: dynamic force, sinusoidal force, harmonic force, force calibration.

1. INTRODUCTION

Established protocols for force transducer calibration are static, whereas many force measurement applications (see e.g. [1]) require accurate knowledge of the force sensing system's dynamic response. This has led to efforts at national metrology institutes [2, 3, 4] to provide dynamic calibration of force transducers, with recent reports [5, 6] of traceable sinusoidal calibrations based on accelerated masses. In this method a body of known mass is affixed to a force transducer to be calibrated, and the two objects are accelerated together sinusoidally. The acceleration is measured, and the product of this acceleration with the known mass gives the force being applied to the transducer. We report here the implementation of such a system at the National Institute of Standards and Technology (NIST), U.S.A., designed for calibration at frequencies up to 2 kHz and with forces up to 2 kN. We describe the uncertainty components for calibrations performed with this system, and show example calibration measurements of a strain-gauge-based transducer.

2. CALIBRATION SYSTEM

A diagram of the calibration system is provided in Fig. 1. The system presented here is the current realization of the system previously described in [7]. The transducer under test is secured to the table of an electrodynamic shaker, with the sensing or "live" end (for transducers that have such a distinction) away from the table; to this is attached a calibration mass. A sinusoidal signal is provided to an amplifier by a signal generator, which in turn drives the shaker at a prescribed frequency and amplitude. The electrodynamic shaker is capable of producing a maximum force of 2 kN over the range of 10 Hz to 4 kHz.

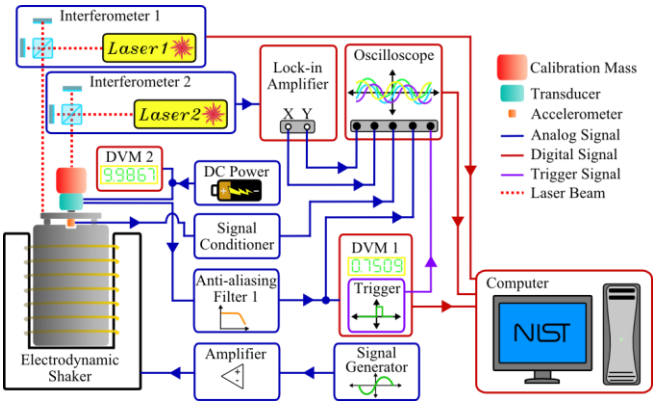

Fig. 1. Schematic diagram of experimental system.

For the majority of transducers, this applied force gives rise to an output voltage, which is the indicator of the force. For strain-gauge-based transducers, the measured output voltage is produced by a strain gauge resistor bridge circuit, which is proportional to the differential change in resistance of strain gauges and to the bridge excitation voltage. The output of the transducer and the excitation voltage are recorded with fast-sampling DC voltmeters (Agilent Technologies 3458A and 34411A respectively) [8]. The transducer output voltage is sampled simultaneously with the position of the calibration mass, which is measured by means of laser vibrometry, with two vibrometers incorporated in the system. The vibrometers can each be configured to make absolute measurements of the top mass motion (i.e. motion relative to a stationary reference mirror), or measurements of the relative motion between two points in the calibration assembly.

3. UNCERTAINTY EVALUATION

Each suspected source of possible significant uncertainty is evaluated by measurement or estimated by calculation. The results are summarized in Tables 1 and 2. In detail, the uncertainty depends on the specific operating point (frequency, force, calibration mass) and the properties of the transducer under calibration. The largest source of uncertainty is angular motion (rocking) of the shaker-transducer-mass assembly. For low-voltage-output transducers, the uncertainty of the voltmeter measurement of the transducer output is also significant.

Table 1. Relative uncertainties for the largest force uncertainty components. All listed components are evaluated by type B methods.

Force uncertainty source	Standard uncertainty [N/N]
Angular motion	3.0×10^{-2} - 1.3×10^{-3}
Optical platform vibrations	2.4×10^{-3} - 3.0×10^{-5}
Vibrometer resolution	1.2×10^{-3} - 3.0×10^{-7}
Elastic wave dynamics	1.2×10^{-3} - 1.7×10^{-5}

Table 2. Relative uncertainties for largest voltage uncertainty components. The first two listed components are type B, while the third (anti-aliasing filter gain) is evaluated by a type A method.

Voltage uncertainty source	Standard uncertainty [V/V]
DVM uncertainty for transducer output voltage (0.1 mV – 10 mV)	2.4×10^{-3} - 3.9×10^{-5}
Off-axis loading	2.5×10^{-4}
Anti-aliasing filter gain	2.1×10^{-4}

3.1 Angular motion

The largest source of uncertainty in the acceleration (and hence the applied force) is due to tilting (rocking) of the calibration assembly, and this is in general a function of frequency. A tilt angle β causes a relative displacement error $\overline{e_{ang}}$ of

$$\overline{e_{ang}} \cong \frac{\epsilon_0 + \delta y}{\delta z}\beta + \frac{\delta z - D}{\delta z}(\beta^2 - \beta\theta) \ , \qquad (1)$$

where ϵ_0 is the initial distance of the measurement spot from the geometric center of the calibration mass surface, δz is the axial (intentional) displacement of the calibration mass, δy is the transverse (undesired) displacement of the calibration mass, D is the path distance from the measurement spot to the photodetector, and θ is the misalignment of the incident laser beam relative to the calibration mass surface normal. The geometry is illustrated in Fig. 2.

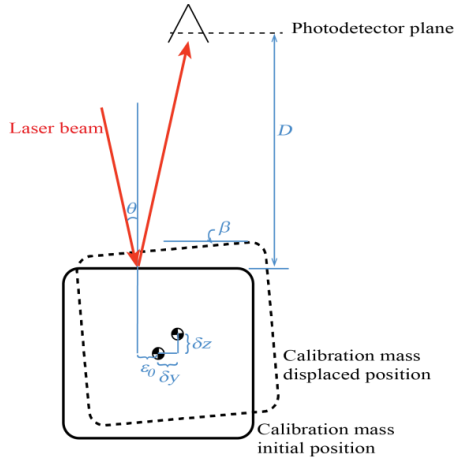

Fig. 2. Angles and displacements involved in calibration mass angular motion.

The tilt angle β was determined by calibrating the variation in interference signal strength with target reflector angle, using a finely-adjustable mirror as the target reflector. This calibration allowed the tilt angle to be determined in-situ during calibration measurements by monitoring the variation in interference signal strength. However it did not allow correction for the effect of tilt, in the first place because the values of θ and ϵ_0 are unknown, and in the second place because the sign of the first term in (1) relative to the true displacement was not determined. For each frequency, these three points define a plane and allow the maximum angle to be calculated. The angle was found not to exceed 7.0×10^{-5} rad, varying non-motonically with frequency according to the dynamical behavior of the calibration stack. ϵ_0 is less than 0.5 mm for calibration measurements made so far, and measurement of $\delta y/\delta z$ found this ratio to be less than or equal to 0.1. A pinhole used in the alignment procedure keeps angle θ below 1.5×10^{-4} rad. The path length D is 1.4 m and the axial displacement amplitude δz ranges from 1 mm to 300 nm.

Thus the dominant terms in (1) are $(\epsilon_0/\delta z)\beta$ and $(D/\delta z)\beta\theta$. The value of β varies with frequency and calibration mass, and the maximum values do not occur at the highest frequencies (where δz is smallest). The resulting uncertainty contribution ranges from 1.3×10^{-3} to 3.0×10^{-2}, where we have assumed a uniform distribution and thus divided the maximal value at each operating point (frequency, displacement amplitude, calibration mass) by $\sqrt{3}$ [9] .

To date we have used variation of the calibration mass to get low-uncertainty calibration measurements at all frequencies, as β at a given frequency varies with the calibration mass. Other means to reduce this uncertainty include improving the precision of alignment, i.e. reducing the possible size of ϵ_0 and θ, averaging measurements of the top mass acceleration made at multiple locations, and structural improvements such as bearings to reduce (or practically eliminate) tilt.

3.2 Vibration of the Interferometer Platform

Vertical motion of the interferometer platform affects the interferometer measurement arm length in the same way as motion of the calibration mass, and so will erroneously be interpreted as motion of the calibration mass[1]. A vibration isolation system is used to minimize platform vibrations. The relative displacement error $\overline{e_{vib}}$ due to interferometer platform vibrations is a function of frequency and is given by

$$\overline{e_{vib}} = \frac{x_b\, T_{plat}(f)}{x_c} \ , \qquad (2)$$

where x_b is the displacement of the shaker table, x_c is the displacement of the calibration mass, and $T_{plat}(f)$ is the experimentally measured transmission coefficient between the shaker table and the optical platform. The transfer function from the shaker table to the interferometer platform was measured using accelerometers mounted at both

[1] This does not apply to differential measurements between two points on the calibration stack.

locations, for two different transducer-mass combinations. For most of the calibration frequency range, the transmission coefficient was below 0.1 %. At particular frequencies (believed to be resonance frequencies of the frame supporting the optical platform), the relative amplitude was as large as 0.25%. As there will be some dependence of $T_{plat}(f)$ on the shaker acceleration amplitude and the combined mass of the calibration stack components, this is taken to be the 1-sigma width of a Gaussian probability distribution. We note that platform vibrations could be measured in real time during calibration measurements and corrected for, thus greatly reducing this uncertainty component.

3.3 Vibrometer Resolution

The specified displacement resolution of vibrometer 1 (Agilent Technologies 5517DL + 10715A + N1231B) is 0.15 nm. The resolution of vibrometer 2 (custom-assembled) was measured to be below 1 nm/Hz$^{1/2}$ throughout the calibration range of the apparatus, with the largest values at low frequencies where the calibration mass displacements are also large. This measurement was done by reorienting an aiming mirror that normally directs the target beam towards the shaker table, so that the beam is instead reflected straight back to the interferometer beamsplitter. This measurement captures all sources of interferometer noise except refractive index fluctuations in the section of the target beampath between the aiming mirror and the calibration mass top surface, and any changes in the mechanical vibration of the aiming mirror caused by its reorientation. The relative uncertainty due to vibrometer resolution is maximum at any frequency for small displacements or accelerations. In Table 1 we assume a minimum acceleration of 1 m/s^2 and a one-second measurement time. We model the uncertainty as uniformly distributed up to the measured or specified resolution.

3.4 Elastic Wave Dynamics

The acceleration of the calibration mass is not exactly uniform throughout the calibration mass, with the variation increasing with drive frequency. The actual force F is proportional to a body-averaged acceleration

$$F = \rho \int_{\text{body}} \boldsymbol{a}(\boldsymbol{r})\, d^3\boldsymbol{r}\,, \qquad (3)$$

where $\boldsymbol{a}$ is the acceleration vector at position $\boldsymbol{r}$ and we have assumed the density ρ is uniform. However the acceleration is measured at one point on the calibration mass surface with a laser vibrometer, and thus the measured acceleration differs from the body-average. A correction factor to account for the internal dynamics of the calibration mass was determined using finite-element analysis (the details of the analysis will be reported elsewhere) and was found to lie between 0.3 % and 2 % at the maximum calibration frequency of 2 kHz, for the range of calibration masses used (1 kg to 10 kg). The uncertainty is near 10 % of the correction factor, dominated by uncertainty in the calibration mass material properties, which were taken from tabulated data. A uniform distribution is assumed for this uncertainty component at each operating point (frequency, calibration mass).

3.5 Voltmeter Uncertainty

The uncertainty in the DVM voltage measurement is a function of the signal amplitude, sampling frequency, sample aperture, averaging time and additional DVM settings. For the settings used for the calibration measurements reported in the next section, the manufacturer-specified relative uncertainty is 6.8×10^{-5} for a 10 mV signal and 4.2×10^{-3} for a 0.1 mV signal. These are taken as maximal values of a uniform distribution.

3.6 Additional Sources of Uncertainty

Static and dynamic misalignment combine with the transducer's sensitivity to moments and transverse forces to cause error; in our system this results in an uncertainty up to 2.5 parts in 10^4 for transducers with transverse force sensitivity $\leq$ 0.25 % of the axial sensitivity and a moment sensitivity (relative to the axial sensitivity) $\leq$ 0.01 %/mm. Repeatability in the measured stability of the gain of the anti-aliasing filter used was within 2.1 parts in 10^4. Other sources of uncertainty evaluated, and found to be below 1 part in 10^4 included mass measurement uncertainty, aerodynamic drag, static alignment effects on the measured acceleration, and uncertainty of the excitation voltage measurement. In a calibration of a transducer's response, repeatability of the transducer's behavior (including mounting effects) is an additional uncertainty component to be measured and combined with the calibration measurement uncertainty.

4. EXAMPLE CALIBRATION

4.1 Calibration Measurements

The performance of the system is demonstrated by example calibration measurements on a strain-gauge-based transducer of 1.3 kN capacity. The static sensitivity of the transducer used is 2.098 mV/V, with a static nonlinearity of 0.026 % in tension and -0.004 % in compression. A 10-Volt DC bridge excitation voltage was used. Calibration measurements were performed spanning the range 100 Hz to

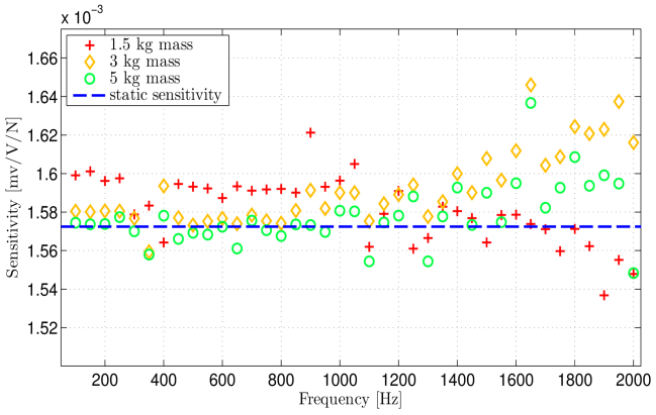

Fig. 3. Measured sensitivity amplitude of 1.3 kN strain-gauge force transducer.

2 kHz at a constant nominal calibration mass acceleration amplitude of 50 m/s^2 (except below 200 Hz where the acceleration amplitude was 10 m/s^2) and with varying calibration mass values. The complex sensitivity at each frequency is determined as the ratio of the Fourier transforms of the transducer output voltage waveform and the applied force waveform. The measured sensitivity amplitude is shown in Fig. 3. In general the sensitivity is expected to be a function of the external mass connected to the transducer; this is due to the inertial force offset due to acceleration of internal mass in the transducer. As the connected external mass is increased, the sensitivity approaches a limiting curve. The sensitivity as $f \rightarrow 0$ in the high-calibration-mass limit agreed with the static sensitivity. The overall expanded uncertainty (k = 2) for the measured sensitivity amplitude at each calibration frequency is provided in Table 3. The dominant contributor to uncertainties above 1 % is off-axis motions of the calibration assembly. As shown in the table, by using two or more calibration masses the transducer is calibrated over the full frequency range with an expanded uncertainty of 1.5 % or less at each frequency. For a given transducer and calibration mass, frequencies with large off-axis motion can be checked in a pre-calibration frequency sweep.

Table 3. Expanded relative uncertainties (k = 2) for sensitivity measurements on a 1.3 kN strain-gauge force transducer using different calibration masses. Points with uncertainty ≥ 1 % are indicated in **boldface**.

Frequency [Hz]	1.5 kg mass	3 kg mass	5 kg mass
100	0.0046	0.0053	0.0032
150	0.0051	0.0039	0.0037
200	0.0042	0.0038	0.0038
250	0.0044	0.0044	0.0044
300	0.0049	0.0050	0.0047
350	**0.0128**	**0.0106**	0.0079
400	**0.0125**	0.0098	0.0068
450		0.0073	0.0066
500	0.0070	0.0069	0.0073
550	0.0074	0.0073	0.0073
600	0.0079	0.0076	0.0082
650	**0.0145**	0.0093	**0.0299**
700	0.0080	0.0081	0.0088
750	0.0082	0.0085	**0.0123**
800	0.0083	0.0094	**0.0113**
850	0.0084	**0.0178**	**0.0129**
900	0.0086	**0.0166**	0.0090
950	0.0087	**0.0120**	**0.0148**
1000	0.0091	**0.0165**	**0.0286**
1050	0.0099	**0.0178**	**0.0307**
1100	**0.0102**	**0.0188**	**0.0326**
1150	**0.0125**	**0.0172**	**0.0283**
1200	**0.0102**	**0.0151**	**0.0226**
1250	**0.0109**	**0.0179**	**0.0284**
1300	**0.0124**	**0.0221**	**0.0357**
1350	**0.0117**	**0.0187**	**0.0276**
1400	**0.0105**	**0.0149**	**0.0187**
1450	**0.0111**	**0.0169**	**0.0224**
1500	**0.0116**	**0.0194**	**0.0270**
1550	**0.0124**	**0.0225**	**0.0330**
1600	**0.0135**	**0.0269**	**0.0405**
1650	**0.0139**	**0.0263**	**0.0388**
1700	**0.0134**	**0.0270**	**0.0375**
1750	**0.0127**	**0.0241**	**0.0284**
1800	**0.0116**	**0.0247**	**0.0230**
1850	**0.0125**	**0.0292**	**0.0248**
1900	**0.0131**	**0.0341**	**0.0312**
1950	**0.0147**	**0.0343**	**0.0264**
2000	**0.0145**	**0.0340**	**0.0246**

4.2 Transducer Model Parameters

A force transducer can be modeled as two lumped masses connected by a linear spring and damper, as depicted in Fig. 4. Values of the model parameters m_s, k_s and c_s can be deduced from the observed dynamic behavior of the transducer. The masses m_p and m_s are accelerated together, and thus the internal force applied to the transducer spring and damper is related to the external force $f_{ext} = m_p \ddot{x}_p$ by

$$f_{int} = -(k_s z + c_s \dot{z}) = f_{ext} \frac{m_p + m_s}{m_p}, \quad (4)$$

or in the frequency domain

$$f_{int} = -(k_s + i\,\omega\, c_s) Z = f_{ext} \frac{m_p + m_s}{m_p}. \quad (5)$$

The transducer output signal is modelled as being proportional to the force applied to the spring, $k_s Z$, so as $\omega \rightarrow 0$, the sensitivity is proportional to $f_{ext} \frac{m_p + m_s}{m_p}$. This variation in sensitivity with calibration mass is evident in fig. 3. From such data we can determine m_s such that the corrected sensitivity as $\omega \rightarrow 0$ is independent of m_p. For the transducer used in this example calibration, m_s is determined to be 0.015 ± 0.0042 kg (k = 1). The equation of motion for the combined top mass $m_p + m_s$ can be written as

$$(m_p + m_s)\ddot{x}_p + c_s(\dot{x}_p - \dot{x}_b) + k_s(x_p - x_b) = 0, \quad (6)$$

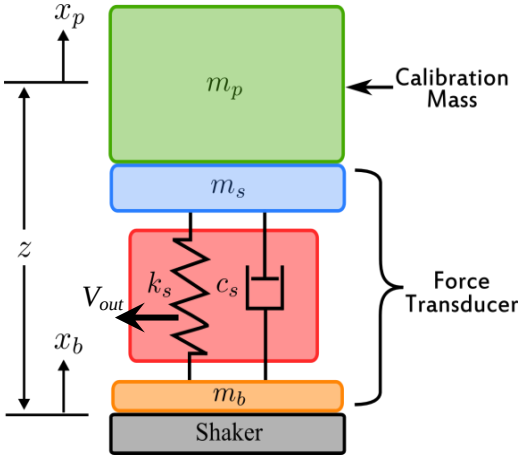

Fig. 4. Single-degree-of-freedom model of the force transducer in the calibration assembly. m_p is the calibration mass, m_s is the top mass of the transducer, m_b is the bottom mass of the transducer, k_s is the stiffness of the transducer and c_s is the damping constant of the transducer. The transducer output voltage is proportional to the extension of spring k_s (and thus to the force applied to this spring).

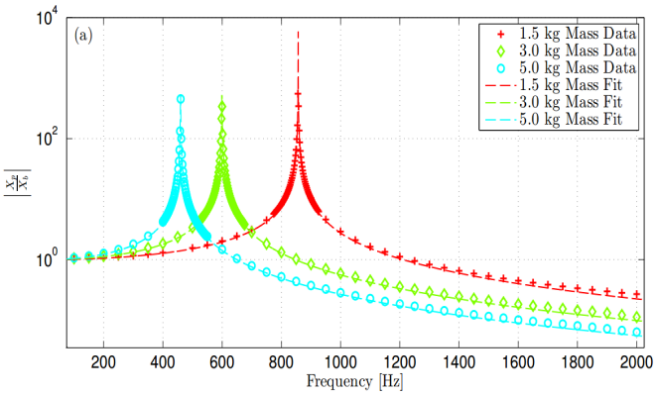

Fig. 5. Observed calibration stack mechanical response for different calibration mass values.

or in the frequency domain as

$$\frac{X_p}{X_b} = \frac{k_s + ic_s\omega}{-(m_p+m_s)\omega^2 + ic_s\omega + k_s} \quad (7)$$

$$= \frac{\omega_n^2 + i2\zeta\omega_n\omega}{\omega_n^2 - \omega^2 + i2\zeta\omega_n\omega}, \quad (8)$$

$$\left|\frac{X_p}{X_b}\right| = \left[\frac{\omega_n^4 + (2\zeta\omega_n\omega)^2}{(\omega_n^2 - \omega^2)^2 + (2\zeta\omega_n\omega)^2}\right]^{1/2}, \quad (9)$$

Where $\omega_n = \sqrt{k_s/(m_p + m_s)}$ and $\zeta = c_s/2(m_p + m_s)\omega_n$. In Fig. 5 we plot the measured mechanical response of the stack for three different calibration mass values m_p. In Table 4 we list resonant frequencies and damping ratios determined by least-squares fitting (9) to these plots. From these we in turn determine the stiffness k_s and damping coefficient c_s according to

$$k_s = (m_p + m_s)\omega_n^2 \cong (m_p + m_s)\frac{\omega_{res}^2}{1-\zeta^2}, \quad (10)$$

$$c_s = 2\zeta(m_p + m_s)\omega_n \cong 2\zeta(m_p + m_s)\frac{\omega_{res}}{\sqrt{1-\zeta^2}}. \quad (11)$$

These values are given in Table 4. The relatively large variation in the determined damping coefficient c_s suggests that the damping model used (linear damping with a frequency-independent damping coefficient) is probably insufficient.

Table 4. Fitted resonant frequencies and damping ratios to the frequency response functions plotted in Fig. 4, and corresponding transducer model parameter values. Uncertainties represent 1 standard deviation.

Calibration mass m_p [kg]	Resonant frequency $\omega_{res}/2\pi$ [Hz]	Damping ratio ζ $\times 10^4$	Stiffness k_s $\times 10^{-7}$ [N/m]	Damping constant c_s [kg/s]
1.43476 ± 4.2×10^{-5}	856.76 ± 0.10	0.02 ± 46.65	4.201 ± 0.012	0.03 ± 77.0
2.95243 ± 8.7×10^{-5}	599.35 ± 0.11	9.53 ± 2.55	4.208 ± 0.060	21.3 ± 5.7
5.02395 ± 1.48×10^{-4}	459.74 ± 0.13	9.35 ± 2.27	4.205 ± 0.039	27.2 ± 6.6

5. CONCLUSION

We have described the sinusoidal force calibration system presently implemented in the force calibration labs at NIST, and reported calibration measurements demonstrating the capability of the system to perform dynamic calibration of force transducers. Work is presently underway to reduce the largest uncertainty components in the system and thereby improve the calibration accuracy.

ACKNOWLEDGMENTS

We thank John Bankert (University of Maryland) for finite-element evaluation of the effect of dynamic elasticity in calibration masses. NV acknowledges the support of a NIST-NRC fellowship.

REFERENCES

[1] J. Hjelmgren, *Dynamic measurement of force – a literature survey*, SP Report 2002:27, ISBN 91-7848-918-0.

[2] M. Dixon, "A traceable dynamic force transducer", *Experimental Mechanics*,vol. 30, no. 2, pp. 152-157, 1990.

[3] R. Kumme, *Investigation of a primary method for a dynamic calibration of force measuring instruments: a contribution to reduce the measuring uncertainty* (*Untersuchungen eines direkten Verfahrens zur dynamischen Kalibrierung von Kraftmeßgeräten – ein Beitrag zur Verringerung der Meßunsicherheit*), Doctoral Thesis TU Braunschweig, PTB-Bericht MA-48, 1996.

[4] K. Ueda and A. Umeda, "Evaluation of force transducers dynamic characteristic by impact", *XIII IMEKO World Congress*, pp. 265-270, 1994.

[5] C. Schlegel, G. Kieckenap, B. Glöckner, A. Buß, and R. Kumme, "Traceable periodic force calibration," *Metrologia*, vol. 49, no. 3, pp. 224–235, 2012.

[6] N. Medina N. and J. de Vicente, "Force Sensor Characterization Under Sinusoidal Excitations", *Sensors*, vol. 14, no. 10, pp. 18454-18473, 2014.

[7] A. Chijioke, "NIST 1-Kilonewton Sine Force Calibration System," *Joint IMEKO International TC3, TC5 and TC22 Conference 2014*, 2014.

[8] Certain commercial equipment, instruments, or materials are identified in this article in order to describe the experimental procedure adequately. Such identification is not intended to imply recommendation or endorsement by the National Institute of Standards and Technology, nor is it intended to imply that the materials or equipment identified are necessarily the best available for the purpose.

[9] ISO, *Guide to the Expression of Uncertainty in Measurement*, prepared by ISO Technical Advisory Group 4 (TAG 4), Working Ground 3 (WG 3), October 1993.